Stretchable Heater Using Ligand-Exchanged Silver Nanowire Nanocomposite for Wearable Articular Thermotherapy

Suji Choi,[†,‡,#] Jinkyung Park,[†,§,#] Wonji Hyun,[†,‡,#] Jangwon Kim,[†,‡] Jaemin Kim,[†,‡] Young Bum Lee,[†,‡] Changyeong Song,[†,‡] Hye Jin Hwang,[⊥] Ji Hoon Kim,[∥] Taeghwan Hyeon,[*,†,‡,§] and Dae-Hyeong Kim[*,†,‡]

[†]Center for Nanoparticle Research, Institute for Basic Science (IBS), Seoul 151—742, Republic of Korea, [‡]School of Chemical and Biological Engineering, Institute of Chemical Processes, Seoul National University, Seoul 151—742, Republic of Korea, [§]Graduate School of Convergence Science and Technology, Seoul National University, Suwon, Gyeonggi-do 443—270, Republic of Korea, [⊥]Division of Cardiology, Beth Israel Deaconess Medical Center, Harvard Medical School, Boston, Massachusetts 02215, United States, and [∥]School of Mechanical Engineering, Pusan National University, Busan 609—735, Republic of Korea. [#]These authors contributed equally to this work.

ABSTRACT Thermal therapy is one of the most popular physiotherapies and it is particularly useful for treating joint injuries. Conventional devices adapted for thermal therapy including heat packs and wraps have often caused discomfort to their wearers because of their rigidity and heavy weight. In our study, we developed a soft, thin, and stretchable heater by using a nanocomposite of silver nanowires and a thermoplastic elastomer. A ligand exchange reaction enabled the formation of a highly conductive and homogeneous nanocomposite. By patterning the nanocomposite with serpentine-mesh structures, conformal lamination of devices on curvilinear joints and effective heat transfer even during motion were achieved. The combination of homogeneous conductive elastomer, stretchable design, and a custom-designed electronic band created a novel wearable system for long-term, continuous articular thermotherapy.

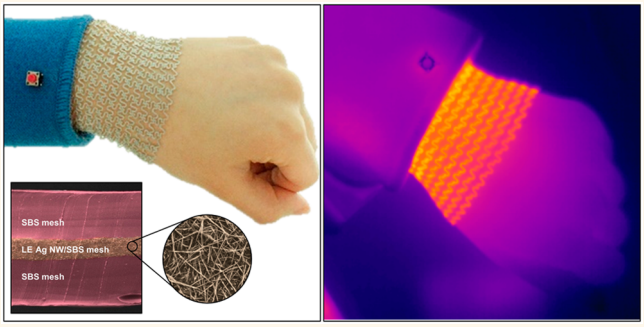

KEYWORDS: silver nanowires · ligand exchange · stretchable heater · wearable electronics · thermotherapy

Joints in the human body are frequently injured due to obesity, occupational overuse, or aging. The joint injuries tend to cause many symptoms such as pain, swelling, muscle weakness, and numbness.[1−5] The thermal therapy is one of the classic physiotherapies used in orthopedics to alleviate these symptoms. Its physiological effects include thermal expansion of the vascular systems (increased blood flow) and their surrounding collagen tissues, thereby relieving pain and reducing joint stiffness.[6,7] There are several conventional heat therapy methods, such as heat packs or wraps:[8,9] the heat packs are heavy and bulky, and another downside is that it is difficult to control their temperature; the heating wraps, whose temperatures are controlled by the joule heating of electrodes and resistors, are relatively thin but, their wearability is still an issue mainly caused by their mechanical rigidity and weight. While continuous point-of-care thermal treatments maximize the therapeutic effects, the technical drawbacks of currently available heat wraps and packs limit their uses mostly in hospitals. Consequently, the development of the stretchable and wearable heating devices in a portable form is highly desired.

To date, there have been several reports on materials and design of stretchable electrodes that can be used as heating elements based on the joule heating. Noteworthy examples include stretchable metal electrodes,[10−12] ultralong percolated carbon nanotubes (CNTs) embedded in elastomers,[13,14] silver flakes chemically bonded with CNTs in polymeric media,[15,16] electrospun rubber fibers with percolation of silver nanoparticles,[17] multilayers of gold nanosheet electrode on a

* Address correspondences to dkim98@snu.ac.kr, thyeon@snu.ac.kr.

Received for review May 8, 2015 and accepted May 30, 2015.

Published online May 31, 2015
10.1021/acsnano.5b02790

rubber substrate,[18] and gold-nanoparticle-based conductive elastomer made through self-assembly.[19] Although each of them has demonstrated some kind of interesting feature, a cheap and simple conductive elastomer that can be easily patterned and processed is still required to be developed. Silver nanowires (Ag NWs) have been recognized as a potential candidate[20−23] because they have higher conductivity than CNTs, and are cheaper than gold. Their one-dimensional wire structure is better to form electrical percolation networks than particles or flakes, and can maintain good conductivity under deformation, especially when stretched. However, an aqueous solution of as-synthesized Ag NWs cannot be mixed homogeneously with many organic-phase elastomers. In the previous applications, Ag NW networks were filtrated and transferred[20,24] or Ag NWs were dip-coated and sprayed on substrate,[25,26] in which the postdeposition processing to define various patterns was difficult.

Here, we present a soft and stretchable heating element that is lightweight and thin, and is conformally integrated with the human joints and the skin for effective heat transfer and thermotherapy. The heater is composed of highly conductive Ag NW/elastomer nanocomposite. The ligand exchange (LE) of Ag NWs allows the nanowires to be homogeneously dispersed in the elastomeric media. This excellent homogeneity leads to mechanically and electrically uniform characteristics and processability of the composite into various patterns, which enables reliable, large-area heating over the entire joint surfaces. The heater is operated by a custom-made electronic band equipped with a battery, a microcontroller, and other circuits, allowing users to remain mobile. The softness of the heater provides maximum comfort, system robustness, and effective thermo-therapies even under joint flexion or muscle extension.

RESULTS AND DISCUSSION

For the synthesis of Ag NWs, a modified seed-mediated polyol process is used.[27,28] The as-synthesized Ag NWs (Supporting Information Figure S1a) are initially dispersed in a polar solvent because of the polyvinylpyrrolidone (PVP) ligands. The average diameter and length are ~150 nm and ~30 μm, respectively (Supporting Information Figure S1b). To achieve stable, uniform, and rapid heating during repeated deformations,[29,30] it is essential to use a homogeneous composite of Ag NWs and elastomer. Most elastomers, however, are only compatible with nonpolar solvents. Among various elastomers, we focus on styrene−butadiene−styrene (SBS) thermoplastic elastomer, which has high elasticity because of its physically cross-linked structures.[31] For homogeneous dispersion of Ag NWs in the organic-phase SBS solution, ligand exchange is necessary; the LE process is schematically illustrated in Figure 1a. The image on the right of Figure 1a shows Ag NWs in toluene after LE, where the PVP ligands are partially exchanged with hexylamine (HAm) using $NOBF_4$.[32] The scanning electron microscope (SEM) image in Figure 1b shows the LE Ag NWs in a magnified view. Zeta-potential measurements show that the surface charge of Ag NWs is positively shifted during the LE reaction (Figure 1c). The presence of HAm is confirmed by the increasing peak intensities of the N−H stretching bond (3400−3250 cm^{-1}) in the FTIR spectra (Figure 1d). Figure 1e shows the thermogravimetric analysis (TGA) results of Ag NWs under a nitrogen environment before

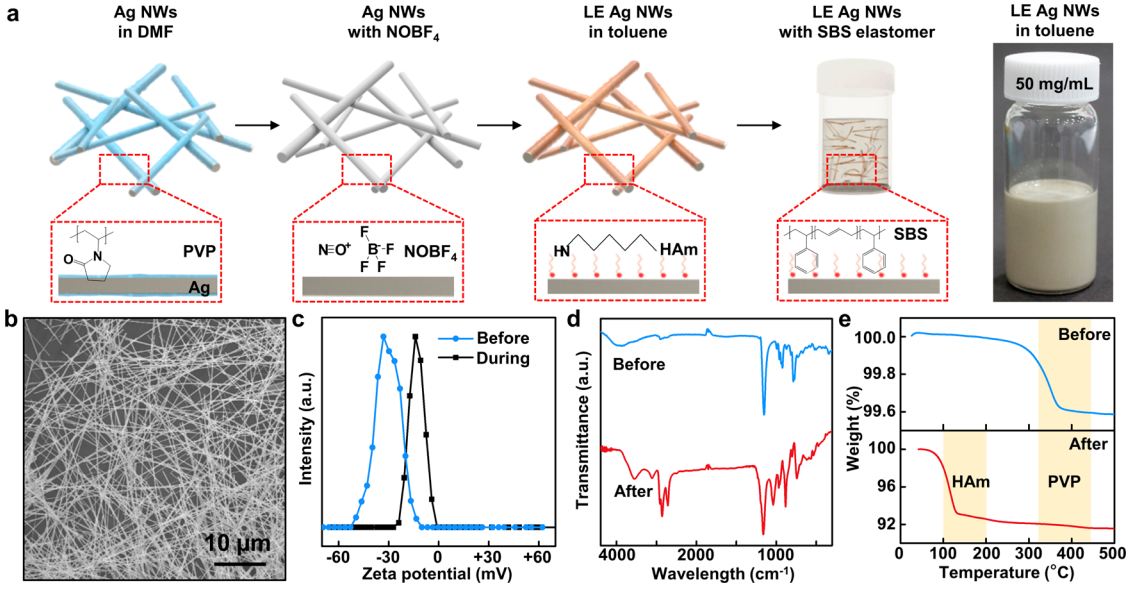

Figure 1. (a) Schematic illustration of the reaction process for ligand-exchanged silver nanowires (LE Ag NWs) and photograph of LE Ag NWs in toluene. (b) SEM image of LE Ag NWs. (c) Zeta-potential measurements of Ag NWs before and during LE process. (d) FTIR spectra (top) before and (bottom) after ligand exchange (LE) of Ag NWs. (e) TGA data of Ag NWs (top) before and (bottom) after LE reaction.

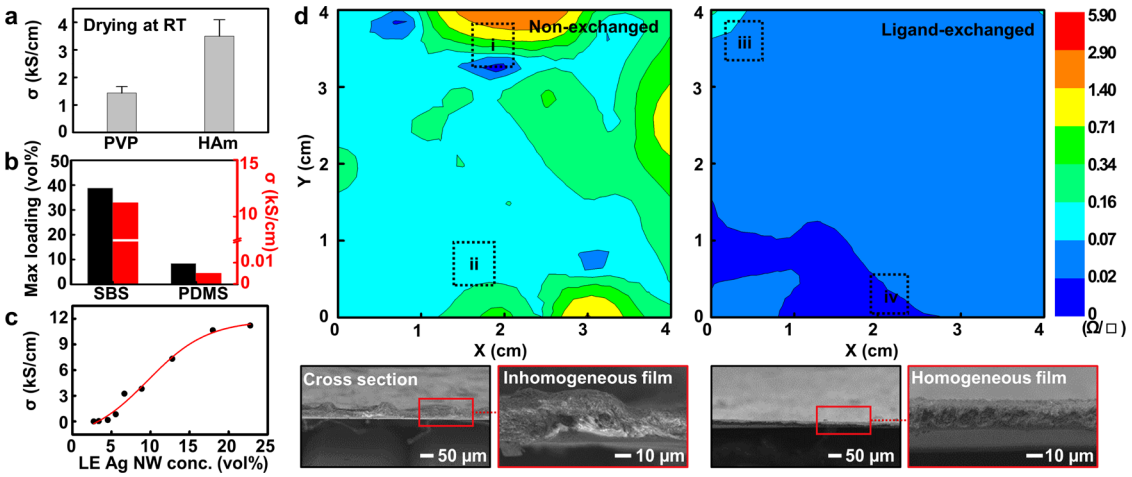

Figure 2. (a) Comparison of conductivity of Ag NWs dried at room temperature before (PVP) and after (HAm) ligand exchange of Ag NWs. (b) Maximum loading amount and corresponding conductivity of Ag NWs in different elastomers: (left) SBS and (right) PDMS. (c) Plot of the electrical conductivity *versus* the amount of LE Ag NWs. (d) (Top) Contour map of sheet resistance and (bottom) cross-sectional SEM images of Ag NW/SBS films (left) without and (right) with ligand exchange. (Top, right) Uniform and low sheet resistance and (bottom, right) uniform film thickness were observed in the LE Ag NW/SBS film.

and after the LE reaction. PVP starts to decompose at ~380 °C,[33] while PVP coated on Ag NWs decomposes at ~350 °C under N_2 atmosphere (Figure 1e). After the LE, the weight loss of ligands on Ag NWs appear in 100−200 and 350 °C, which correspond to the decomposition of HAm and PVP, respectively.[34,35] The weight ratio of HAm to PVP is 75:25.

The LE Ag NWs have higher conductivity than the non-exchanged Ag NWs when they are dried at room temperature (Figure 2a). The higher conductivity of LE Ag NWs is due to the shorter chain length of HAm ligands after LE and thereby lower contact resistance between Ag NWs. This property also improves the conductivity of Ag NWs embedded in SBS even at low annealing temperature below the thermal-degradation temperature. The advantage of a physically cross-linked elastomer like SBS over a chemically cross-linked one like polydimethylsiloxane (PDMS) is the high loading of LE Ag NWs, which can maximize the conductivity of the nanocomposite (Figure 2b). For example, PDMS could not be polymerized under the maximum loading of Ag NWs permitted in SBS (~40 vol %). This high Ag NW loading maximizes the conductivity of the composite. The conductivity of the LE Ag NW/SBS nanocomposite begins to be saturated at ~20 vol %, which we choose as an optimum volume ratio of the constituents for the further processes (Figure 2c). The contour maps in the top row of Figure 2d compare the uniformity of the sheet resistance distribution of non-exchanged Ag NW/SBS (left) and LE Ag NW/SBS (right). LE Ag NW/SBS shows better material properties, *i.e.*, high uniformity and low resistance. The cross-sectional and top-view SEM images (bottom row of Figure 2d and Supporting Information Figure S1c, respectively) confirm the homogeneous dispersion of LE Ag NW/SBS. The top SEM images correspond to the region of small dotted boxes (i−iv) in contour maps.

To maximize the system-level softness and stretchability, we adopt fully serpentine mesh design, which allows conformal integration of the heater on movable joints and provides more comfort and efficient heat conduction.[36] Figure 3a shows a schematic illustration of the fabrication process using prefabricated PDMS molds with serpentine designs (Supporting Information Figure S2a).[37] LE Ag NWs make a homogeneous solution with SBS. It shows better wetting to the PDMS mold than non-exchanged Ag NWs (Supporting Information Figure S2b,c). The heating layer (LE Ag NW/SBS nanocomposite) is sandwiched between the encapsulation layers (*i.e.*, SBS insulation layers), which have slightly larger patterns than the heating layer to seal the edges. The stacked layers are pressed at 100 °C, which welds the layers to form the final serpentine mesh heater.[38] To prevent the thermal decomposition of SBS polymer, all molding processes were conducted under 100 °C.[39,40] A colorized cross-sectional SEM image shows the good interfaces between the layers (Figure 3b). In terms of the mesh design, the higher fill factor is beneficial for more efficient heat transfer (Supporting Information Figure S3),[41] and it does not diminish the stretchability in the biaxial directions (Figure 3c). The final serpentine-mesh heater made from a nanocomposite with a volume ratio of 18/82 (LE Ag NW/SBS) shows a low resistance of ~0.8 Ω. Figure 3d shows the changes in the temperature−time profiles when various input voltages are applied to the mesh heater for ~120 s. Because of the high conductivity, the temperature can be rapidly increased from room temperature to ~40 °C with only an applied voltage of 1.0 V. The stable and fast heating property of the mesh heater is also confirmed by the repetitive on−off cycles with

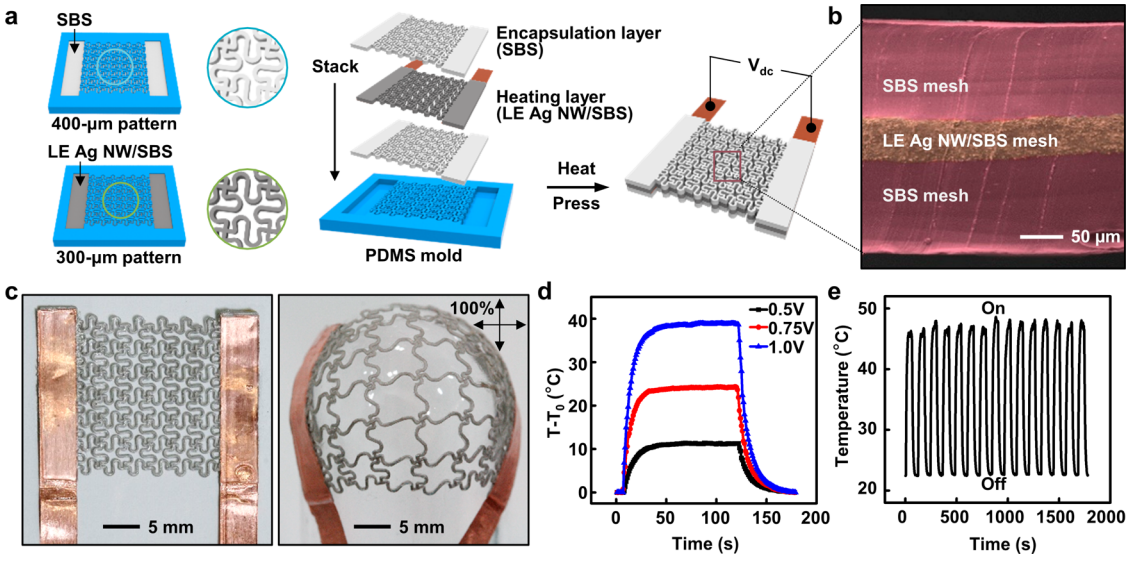

Figure 3. (a) Schematic illustration of the mesh heater fabrication process. The stretchable heater consisted of encapsulation layers (SBS) and a heating layer (LE Ag NW/SBS). Thermal welding with heat and pressure was used to combine and bond each layer. (b) SEM images showing the welded interfaces. (c) Optical image of a final mesh heater (left) before and (right) after biaxial stretching up to ~100%. (d) Temperature profiles under applied voltages of 0.5, 0.75, and 1.0 V on the heater. (e) Stable and fast on/off responses under applied voltage of ~0.5 V.

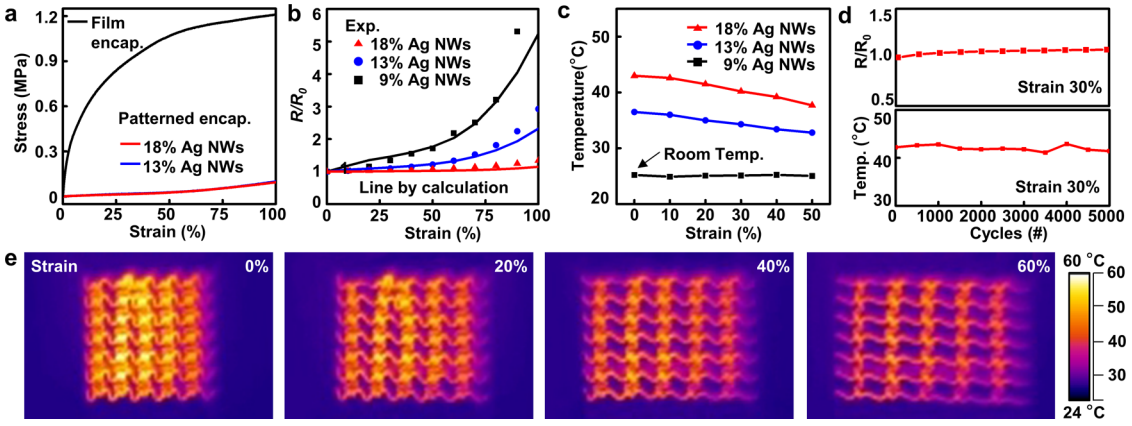

Figure 4. (a) Stress–strain curves of mesh heaters depending on the encapsulation type and Ag NW concentration in the LE Ag NW/SBS mesh layer. Each encapsulation type is illustrated by a photograph in Supporting Information Figure S4a. (b) Experimental (dot) and theoretical (line) values of relative resistance (R/R_0) of LE Ag NW/SBS meshes with different amounts of Ag NWs under tensile strains up to ~100%. (c) Temperature profiles of LE Ag NW/SBS meshes with different amounts of Ag NWs under tensile strains up to ~50% under applied 0.45 V. (d) Cyclic stretching test with applied strain of ~30%. The changes in (top) relative resistance and (bottom) temperature were monitored in the LE Ag NW/SBS mesh with volume ratio of 18/82. (e) Infrared (IR) camera images of meshes at applied strains of 0, 20, 40, and 60% and applied voltage of 0.75 V.

durations of ~60 s under an applied voltage of 0.5 V (Figure 3e).

Figure 4 shows the mechanical, electrical, and thermal characterization of the heaters. Compared with the film-type SBS encapsulation (Supporting Information Figure S4a, left), the patterned SBS encapsulation (Figure S4a, right) induces less stress during stretching regardless of the mixing ratio of LE Ag NW/SBS (18/82 and 13/87) (Figure 4a; black *versus* red and blue lines). The mixing ratios of LE Ag NW/SBS do not also have much influence on the strain distribution, which is explained by the finite element (FE) simulation (Supporting Information Figure S4b). However, the concentration of LE Ag NWs in the heating layer significantly affects the thermo-resistive properties. Figure 4b shows the changes in relative resistance (R/R_0) under different uniaxial tensile strains for the mesh heaters with different LE Ag NW concentrations. The mesh heater with higher LE Ag NW concentration shows more stable values of resistance under the induced strains because of more percolations and fewer disconnections in the conducting paths, which is confirmed by the FE simulations of electrical conduction of the stretched mesh heaters (Figure S4c; see Supporting Information for details).

As for the wearable systems applied in the articular region, the devices should endure the deformation of joints. The strains induced on the wrist and the knee

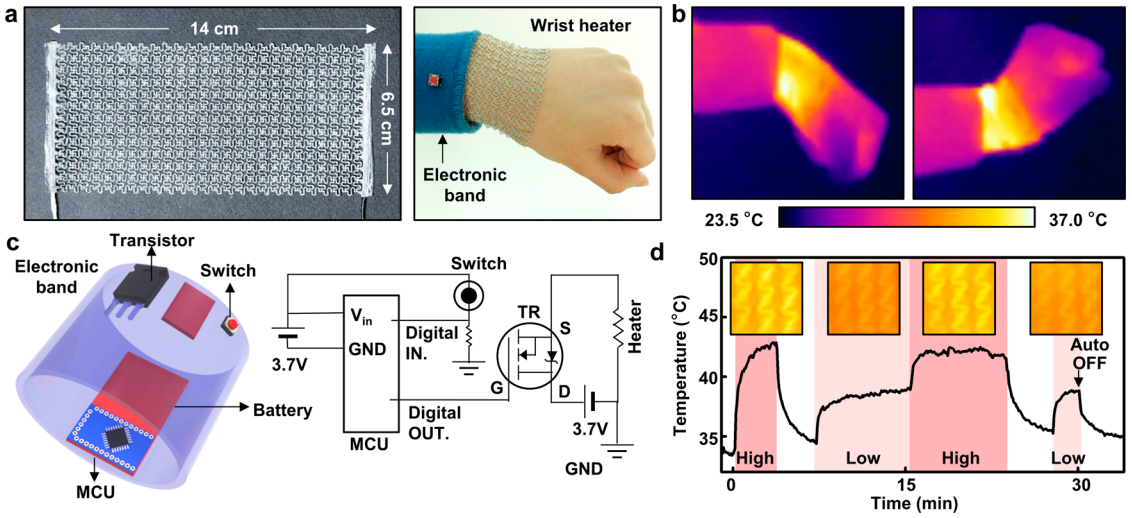

Figure 5. (a) (Left) Image of a large-area stretchable heater designed for the wrist; (right) image of the heater as it was worn on the wrist. The blue strap shows the custom-made electronic band for the power supply and electronic circuits. (b) IR camera images when the wrist moved downward and upward. (c) Schematic illustration showing (left) components of the electronic band and (right) the corresponding circuit diagram. (d) Control of temperature profiles using a custom-made program; the insets show IR camera images obtained under each heating condition.

during flexion or extension are ~17 and ~26% (Supporting Information Figure S5a,b), respectively, which are much below ~50%. On the basis of these observations, the maximum temperature change is measured in the strain range of ~50% and below (Figure 4c). The high percolation of 18 vol % LE Ag NW mesh heater maintains the high current flow and low resistance under the stretched condition, while 9 vol % LE Ag NW mesh heater has the limited percolation and high resistance particularly at the stretched condition. The high temperature heating of the 18 vol % LE Ag NW mesh heater causes the higher heat flux from the heater to the ambient air and thereby the faster cooling than the 9 vol % case. We use the mesh composed of LE Ag NW/SBS with a volume ratio of 18/82 for the cyclic stretching test. Under the induced strains of ~30% over 5000 repetitive cycles, the resistance and joule-heating characteristics remain stable (Figure 4d). Even after the UV exposure for 48 h, the thermal property of the mesh heater is still maintained without significant degradation in heater performance. The stable electrical and mechanical property after the UV exposure is also confirmed by the cyclic stretching test (Supporting Information Figure S6). Figure 4e shows a series of infrared (IR) camera images during the joule heating at an applied voltage of ~0.75 V under uniaxial strains of ~0, ~20, ~40, and ~60%. The air-cooling effect in Figure 4c is also observed in Figure 4e.

When a large-area stretchable mesh heater (14 cm × 6.5 cm; Figure 5a, left) is integrated with a custom-made electronic band (Figure 5a, right), the system becomes portable. The heater size matches the average wrist size of the adult subjects. The mesh heater is safe to use and the test subjects show no rashes or signs of irritation after wearing it for 12 h (Supporting Information Figure S7). Powered by the battery installed in the electronic band, the entire area of the stretchable mesh generates heat. The properties of homogeneity, high conductivity, and softness enable the stretchable heater to heat evenly and maintain conformal contacts with the joint during flexion and extension (IR camera images in Figure 5b). The conducting layer sandwiched between the thin elastomeric encapsulation layers prevents electrical leakage but transfer heat effectively. Figure 5c shows a schematic illustration and the corresponding circuit diagram of the electronic band containing the power supply and the microcontroller unit (MCU). A custom-designed program is installed in the MCU to control the heating modes (Figure S8a and Supporting Information Movie 1). The number of clicks on the switch determines the specific heating mode by modulating the voltage applied to the gate terminal of the transistor through pulse-width modulation (Figure S8b; see Supporting Information for details). The transistor resistance is modified by changing the gate voltage, which controls the electrical current to flow through the heater. Various thermal profiles can be either custom-designed or preprogrammed (Figure 5d). The custom-designed program also would turn the power switch off automatically after 30 min of the operation in order to prevent low-temperature burns (right end of Figure 5d).

Articular thermotherapy induces vasodilation and increases blood flow around the joints, which reduces pain and joint stiffness.[7,42] To achieve adequate therapeutic results, the effective heat transfer from the mesh heater is important. Heat transfer modeling from the mesh heater shows that the overall temperature rises on the skin surface and in the subcutaneous layer by thermal diffusion (Figure 6a and Figure S9a;

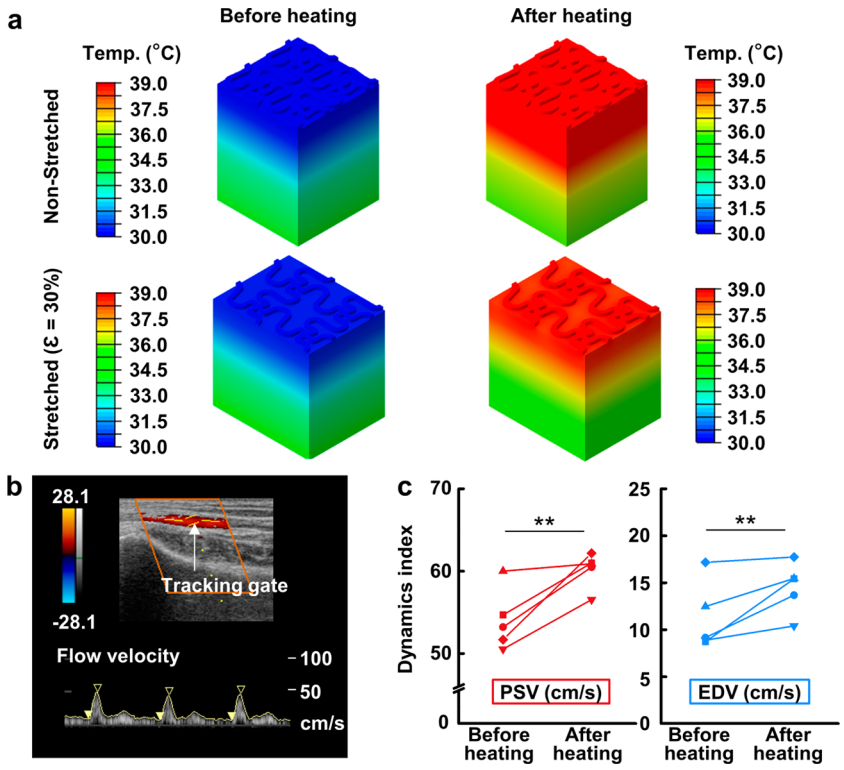

Figure 6. (a) Simulation of three-dimensional temperature distribution from the mesh heater to the subcutaneous layer before heating and after 15 min of heating. (b) A Doppler color image using B-mode ultrasound shows pulsatile blood flow in the radial artery located in the forearm. The blood-flow velocities were measured from a longitudinal duplex Doppler spectral waveform. (c) Comparison of peak systolic velocity (PSV) and end-diastolic velocity (EDV) before and after heating (n = 5). **P < 0.05 with a paired Student's t-test.

see Supporting Information for details).[43] The stretched mesh under the flexed condition (ε = 30%) continues to effectively heat the subcutaneous layer (Supporting Information Figure S9b). The degree of vasodilation, one of the effects of the thermal therapy, is to be estimated by directly measuring blood flow in the radial artery with B-mode ultrasound (Supporting Information Figure S10 and Movie 2).[44] Five healthy adult volunteers participated in the test. The color Doppler imaging (Figure 6b) displays the pulsatile blood flow in the radial artery. The dynamic indices, including the peak systolic velocity (PSV) and the end-diastolic velocity (EDV), are measured directly from the Doppler spectral waveforms at the baseline (initial) and after heating (~40 °C) for 10 min. Warming by the stretchable heater increases PSV from 54.02 ± 1.65 to 60.22 ± 0.96 cm/s (n = 5, P < 0.05; Figure 6c, left) and EDV from 11.28 ± 1.63 to 14.54 ± 1.22 cm/s (n = 5, P < 0.05; Figure 6c, right). These results demonstrate that the blood flow increases by the articular thermal actuation, possibly leading to the pain alleviation and the muscle relaxation.[42,45]

CONCLUSION

In summary, we demonstrate the fabrication and performance of the stretchable heater made of a homogeneous nanocomposite of Ag NWs and SBS elastomer. The high conductivity of the Ag NW/SBS nanocomposite runs the stretchable heater with low input voltages powered by a small battery. Furthermore, the mesh heater has a low system modulus and small changes in resistance under the uniaxial or biaxial strains. The heating profile on the wrist is uniform and stable despite large joint movements. This patterning process is also applicable to larger areas, which would allow the heater to cover knee or other body parts as well. Since the soft stretchable heater makes conformal contact with the skin, the heat transfer to muscles or blood vessels is effective. Integrating the stretchable heater with a custom-made electronic band provides further wearability and makes the system truly portable to perform the point-of-care articular thermotherapy.

METHOD

Synthesis of Ag Nanowires. To synthesize Ag NWs, a modified $CuCl_2$-mediated polyol process was used. After 800 μL of a 4 mM copper chloride solution ($CuCl_2 \cdot 2H_2O$; Aldrich) was added to 130 mL of a 0.034 M PVP solution (average molecular weight, 55 000; Aldrich) in an oil bath (153 °C), 30 mL of 0.094 M silver

nitrate ($AgNO_3$; > 99% purity, Strem Chemicals, Inc.) in an ethylene glycol solution was injected for 25 min. The synthesis reaction lasted 1 h.

Ligand Exchange Reaction of Ag NWs and Preparation of Ag NW/SBS Nanocomposite. First, 0.3 g of Ag NWs was dispersed in 30 mL of dimethylformamide. Next, 30 mL of 0.01 M $NOBF_4$ was added to the Ag NW solution. After 5 min of gentle shaking, 10 mL of hexylamine was added to the reaction solution. The synthesized LE Ag NW solution was purified by ethanol, centrifuged, and redispersed in toluene with a concentration of 50 mg/mL. SBS (KTR-101, Kumho, South Korea) was dissolved in toluene at a weight ratio of 1:10. The LE Ag NW/SBS solution with the appropriate ratio was mixed and dried to form the LE Ag NW/SBS nanocomposite solution.

Characterizations of LE Ag NWs. Fourier-transform infrared (FTIR) spectra were obtained in the transmission mode using the FTIR spectorometer (FT-IR 200, Jasco). The contour map of sheet resistance was measured using the automatic resistivity meter (FPP-5000 4-point probe, Changmin, Co., South Korea). The cross-sectional images were obtained by a scanning electron microscope (SEM; JSM-6701F, JEOL, Japan). The stress−strain curve was measured with a 2 cm × 2 cm heater, using the universal testing machine (Instron5543, Instron).

Fabrication of Stretchable Heater. To produce the heating layer of the stretchable mesh heater, the LE Ag NW/SBS nanocomposite solution was cast on a serpentine-patterned PDMS mold with 300-μm line width and then dried at 60 °C. The encapsulation layer of the heater was formed by the SBS solution cast on a 400-μm line patterned PDMS mold. After heating and the encapsulation layers were demolded, each layer was aligned on the 400-μm patterned PDMS mold and placed on a 130 °C hot plate for 30 min to weld them to each other. The other side of the encapsulation layer was assembled as well after wiring both ends of the mesh with copper wires and conductive paste. The whole size and pattern size of the mesh for wrist band were modified according to the wrist size.

Characterizations of the Stretchable Mesh Heater. The relative resistance under tensile strain were obtained by a parameter analyzer (B1500A, Agilent) with a custom-made *x*-axis motion stage. All thermal properties and images were obtained by an infrared (IR) camera (Thermovision A320, FLIR system, Sweden). The average and maximum temperature were analyzed using the built-in analysis software (FLIR tools, FLIR system, Sweden).

Conflict of Interest: The authors declare no competing financial interest.

Acknowledgment. This work was supported by IBS-R006-D1. This work was also supported by the Seoul National University Research Grant.

Supporting Information Available: Detailed experimental procedure and characterization method, FE model and analysis, skin irritation test, sonography process, SEM images and size distribution histogram, electronic band circuits. Movies 1 and 2 (.avi) showing operation of customized electronic band and blood flow measurement. The Supporting Information is available free of charge on the ACS Publications website at DOI: 10.1021/acsnano.5b02790.

REFERENCES AND NOTES

1. Coggon, D.; Croft, P.; Kellingray, S.; Barrett, D.; McLaren, M.; Cooper, C. Occupational Physical Activities and Osteoarthritis of the Knee. *Arthritis Rheum.* **2000**, *43*, 1443–1449.
2. Loeser, R. F.; Goldring, S. R.; Scanzello, C. R.; Goldring, M. B. Osteoarthritis: A Disease of the Joint as an Organ. *Arthritis Rheum.* **2012**, *64*, 1697–1707.
3. Hartz, A. J.; Fischer, M. E.; Bril, G.; Kelber, S.; Rupley, D.; Oken, B.; Rimm, A. A. The Association of Obesity with Joint Pain and Osteoarthritis in the HANES Data. *J. Chronic Dis.* **1986**, *39*, 311–319.
4. Felson, D. T.; Naimark, A.; Anderson, J.; Kazis, L.; Castelli, W.; Meenan, R. F. The Prevalence of Knee Osteoarthritis in the Elderly. The Framingham Osteoarthritis Study. *Arthritis Rheum.* **1987**, *30*, 914–918.
5. Maghsoudipour, M.; Moghimi, S.; Dehghaan, F.; Rahimpanah, A. Association of Occupational and Non-Occupational Risk Factors with the Prevalence of Work Related Carpal Tunnel Syndrome. *J. Occup. Rehabil.* **2008**, *18*, 152–156.
6. Lehmann, J. F. *Therapeutic Heat and Cold*, 4th ed.; Williams & Wilkins: Baltimore, MD, 1990.
7. Brosseau, L.; Yonge, K. a; Robinson, V.; Marchand, S.; Judd, M.; Wells, G.; Tugwell, P. Thermotherapy for Treatment of Osteoarthritis. *Cochrane Database Syst. Rev.* **2003**, CD004522.
8. Petrofsky, J. S.; Laymon, M.; Lee, H. Effect of Heat and Cold on Tendon Flexibility and Force to Flex the Human Knee. *Med. Sci. Monit.* **2013**, *19*, 661–667.
9. Michlovitz, S.; Hun, L.; Erasala, G. N.; Hengehold, D. a.; Weingand, K. W. Continuous Low-Level Heat Wrap Therapy Is Effective for Treating Wrist Pain. *Arch. Phys. Med. Rehabil.* **2004**, *85*, 1409–1416.
10. Webb, R. C.; Bonifas, A. P.; Behnaz, A.; Zhang, Y.; Yu, K. J.; Cheng, H.; Shi, M.; Bian, Z.; Liu, Z.; Kim, Y.-S.; et al. Ultrathin Conformal Devices for Precise and Continuous Thermal Characterization of Human Skin. *Nat. Mater.* **2013**, *12*, 938–944.
11. Son, D.; Lee, J.; Qiao, S.; Ghaffari, R.; Kim, J.; Lee, J. E.; Song, C.; Kim, S. J.; Lee, D. J.; Jun, S. W.; et al. Multifunctional Wearable Devices for Diagnosis and Therapy of Movement Disorders. *Nat. Nanotechnol.* **2014**, *9*, 397–404.
12. Kim, J.; Lee, M.; Shim, H. J.; Ghaffari, R.; Cho, H. R.; Son, D.; Jung, Y. H.; Soh, M.; Choi, C.; Jung, S.; et al. Stretchable Silicon Nanoribbon Electronics for Skin Prosthesis. *Nat. Commun.* **2014**, *5*, 1–11.
13. Sekitani, T.; Noguchi, Y.; Hata, K.; Fukushima, T.; Aida, T.; Someya, T. A Rubberlike Stretchable Active Matrix Using Elastic Conductors. *Science* **2008**, *321*, 1468–1472.
14. Jung, S.; Kim, J. H.; Kim, J.; Choi, S.; Lee, J.; Park, I.; Hyeon, T.; Kim, D. H. Reverse-Micelle-Induced Porous Pressure-Sensitive Rubber for Wearable Human-Machine Interfaces. *Adv. Mater.* **2014**, *26*, 4825–4830.
15. Chun, K.-Y.; Oh, Y.; Rho, J.; Ahn, J.-H.; Kim, Y.-J.; Choi, H. R.; Baik, S. Highly Conductive, Printable and Stretchable Composite Films of Carbon Nanotubes and Silver. *Nat. Nanotechnol.* **2010**, *5*, 853–857.
16. Ma, R.; Lee, J.; Choi, D.; Moon, H.; Baik, S. Knitted Fabrics Made from Highly Conductive Stretchable Fibers. *Nano Lett.* **2014**, *14*, 1944–1951.
17. Park, M.; Im, J.; Shin, M.; Min, Y.; Park, J. J.; Cho, H.; Park, S.; Shim, M.-B.; Jeon, S.; Chung, D.-Y.; et al. Highly Stretchable Electric Circuits from a Composite Material of Silver Nanoparticles and Elastomeric Fibres. *Nat. Nanotechnol.* **2012**, *7*, 803–809.
18. Moon, G. D.; Lim, G.-H.; Song, J. H.; Shin, M.; Yu, T.; Lim, B.; Jeong, U. Highly Stretchable Patterned Gold Electrodes Made of Au Nanosheets. *Adv. Mater.* **2013**, *25*, 2707–2712.
19. Kim, Y.; Zhu, J.; Yeom, B.; Di Prima, M.; Su, X.; Kim, J.-G.; Yoo, S. J.; Uher, C.; Kotov, N. A. Stretchable Nanoparticle Conductors with Self-Organized Conductive Pathways. *Nature* **2013**, *500*, 59–63.
20. Lee, P.; Lee, J.; Lee, H.; Yeo, J.; Hong, S.; Nam, K. H.; Lee, D.; Lee, S. S.; Ko, S. H. Highly Stretchable and Highly Conductive Metal Electrode by Very Long Metal Nanowire Percolation Network. *Adv. Mater.* **2012**, *24*, 3326–3332.
21. Liang, J.; Li, L.; Niu, X.; Yu, Z.; Pei, Q. Elastomeric Polymer Light-Emitting Devices and Displays. *Nat. Photonics* **2013**, *7*, 817–824.
22. Liang, J.; Li, L.; Tong, K.; Ren, Z.; Hu, W.; Niu, X.; Chen, Y.; Pei, Q. Silver Nanowire Percolation Network Soldered with Graphene Oxide at Room Temperature and Its Application for Fully Stretchable Polymer Light-Emitting Diodes. *ACS Nano* **2014**, *8*, 1590–1600.
23. Hu, L.; Kim, H. S.; Lee, J.; Peumans, P.; Cui, Y. Scalable Coating and Properties of Transparent, Flexible, Silver Nanowire Elecrodes. *ACS Nano* **2010**, *4*, 2955–2963.
24. Amjadi, M.; Pichitpajongkit, A.; Lee, S.; Ryu, S.; Park, I. Highly Stretchable and Sensitive Strain Sensor Based on Silver Nanowire-Elastomer Nanocomposite. *ACS Nano* **2014**, *8*, 5154–5163.

25. Ge, J.; Yao, H. B.; Wang, X.; Ye, Y. D.; Wang, J. L.; Wu, Z. Y.; Liu, J. W.; Fan, F. J.; Gao, H. L.; Zhang, C. L.; et al. Stretchable Conductors Based on Silver Nanowires: Improved Performance through a Binary Network Design. *Angew. Chem., Int. Ed.* **2013**, *52*, 1654–1659.
26. Lee, J.; Lee, I.; Kim, T. S.; Lee, J. Y. Efficient Welding of Silver Nanowire Networks without Post-Processing. *Small* **2013**, *9*, 2887–2894.
27. Korte, K. E.; Skrabalak, S. E.; Xia, Y. Rapid Synthesis of Silver Nanowires through a CuCl- or $CuCl_2$-Mediated Polyol Process. *J. Mater. Chem.* **2008**, *18*, 437.
28. Paul, A.; Zhen, Y. R.; Wang, Y.; Chang, W. S.; Xia, Y.; Nordlander, P.; Link, S. Dye-Assisted Gain of Strongly Confined Surface Plasmon Polaritons in Silver Nanowires. *Nano Lett.* **2014**, *14*, 3628–3633.
29. Hsu, P.; Liu, X.; Liu, C.; Xie, X.; Lee, H. R.; Welch, A. J.; Zhao, T.; Cui, Y. Personal Thermal Management by Metallic Nanowire-Coated Textile. *Nano Lett.* **2015**, *15*, 365–371.
30. Kim, T.; Kim, Y. W.; Lee, H. S.; Kim, H.; Yang, W. S.; Suh, K. S. Uniformly Interconnected Silver-Nanowire Networks for Transparent Film Heaters. *Adv. Funct. Mater.* **2013**, *23*, 1250–1255.
31. Kennedy, J. E.; Higginbotham, C. L. Synthesis and Characterisation of Styrene Butadiene Styrene Based Grafted Copolymers for Use in Potential Biomedical Applications. In *Biomedical Engineering, Trends in Materials Science*; Laskovski, A., Ed.; InTech: Rijeka, Croatia, 2011; pp 465−488.
32. Dong, A.; Ye, X.; Chen, J.; Kang, Y.; Gordon, T.; Kikkawa, J. M.; Murray, C. B. A Generalized Ligand-Exchange Strategy Enabling Sequential Surface Functionalization of Colloidal Nanocrystals. *J. Am. Chem. Soc.* **2011**, *133*, 998–1006.
33. Du, Y. K.; Yang, P.; Mou, Z. G.; Hua, N. P.; Jiang, L. Thermal Decomposition Behaviors of PVP Coated on Platinum Nanoparticles. *J. Appl. Polym. Sci.* **2006**, *99*, 23–26.
34. Witt, E.; Witt, F.; Trautwein, N.; Fenske, D.; Neumann, J.; Borchert, H.; Parisi, J.; Kolny-Olesiak, J. Synthesis of Lead Chalcogenide Nanocrystals and Study of Charge Transfer in Blends of PbSe Nanocrystals and poly(3-Hexylthiophene). *Phys. Chem. Chem. Phys.* **2012**, *14*, 11706–11714.
35. You, T.; Wang, J.; Feng, H.; Chen, K.; Fan, W.; Zhang, C.; Miao, R. The Competition between Template Growth and Catalytic Growth of One-Dimensional ZnS Nanostructures: Nanobelts or Nanowires. *Dalton Trans.* **2013**, *42*, 7724–7730.
36. Kim, D.-H.; Lu, N.; Ma, R.; Kim, Y.-S.; Kim, R.-H.; Wang, S.; Wu, J.; Won, S. M.; Tao, H.; Islam, A.; et al. Epidermal Electronics. *Science* **2011**, *333*, 838–843.
37. Xia, Y.; Whitesides, G. M. Soft Lithography. *Annu. Rev. Mater. Sci.* **1998**, *28*, 153–184.
38. Yousefpour, A.; Hojjati, M.; Immarigeon, J.-P. Fusion Bonding/Welding of Thermoplastic Composites. *J. Thermoplast. Compos. Mater.* **2004**, *17*, 303–341.
39. Xu, J.; Zhang, A.; Zhou, T.; Cao, X.; Xie, Z. A Study on Thermal Oxidation Mechanism of Styrene-Butadiene-Styrene Block Copolymer (SBS). *Polym. Degrad. Stab.* **2007**, *92*, 1682–1691.
40. Hacaloglu, J.; Ersen, T.; Ertugrul, N.; Fares, M. M.; Suzer, S. Pyrolysis Mass Spectrometric Analysis of Styrene-Butadiene Block and Random Copolymers. *Eur. Polym. J.* **1997**, *33*, 199–203.
41. Fan, J. a; Yeo, W.-H.; Su, Y.; Hattori, Y.; Lee, W.; Jung, S.-Y.; Zhang, Y.; Liu, Z.; Cheng, H.; Falgout, L.; et al. Fractal Design Concepts for Stretchable Electronics. *Nat. Commun.* **2014**, *5*, 3266.
42. Oosterveld, F. G. J.; Rasker, J. J. Treating Arthritis with Locally Applied Heat or Cold. *Semin. Arthritis Rheum.* **1994**, *24*, 82–90.
43. Hattori, Y.; Falgout, L.; Lee, W.; Jung, S.-Y.; Poon, E.; Lee, J. W.; Na, I.; Geisler, A.; Sadhwani, D.; Zhang, Y.; et al. Multifunctional Skin-Like Electronics for Quantitative, Clinical Monitoring of Cutaneous Wound Healing. *Adv. Healthc. Mater.* **2014**, *3*, 1597–1607.
44. Lockhart, M. E.; Robbin, M. L.; Allon, M. Preoperative Sonographic Radial Artery Evaluation and Correlation with Subsequent Radiocephalic Fistula Outcome. *J. Ultrasound Med.* **2004**, *23*, 161–168.
45. Abramson, D. I.; Belly, Y.; Tuck, S.; Mitchell, R.; Chandrasekharappa, G. Changes In Blood Flow, Oxygen Uptake and Tissue Temperatures Produced by Therapeutic Physical Agents: III. Effect of Indirect or Reflex Vasodilatation. *Am. J. Phys. Med.* **1961**, *40*, 5–13.